Photocatalytic Selective Oxidation of 5-(Hydroxymethyl)-2-furaldehyde to 2,5-Furandicarbaldehyde in Water by Using Anatase, Rutile, and Brookite TiO$_2$ Nanoparticles

Sedat Yurdakal,[†,*] Bilge Sina Tek,[†] Oğuzhan Alagöz,[†] Vincenzo Augugliaro,[‡,*] Vittorio Loddo,[‡] Giovanni Palmisano,[‡] and Leonardo Palmisano[‡]
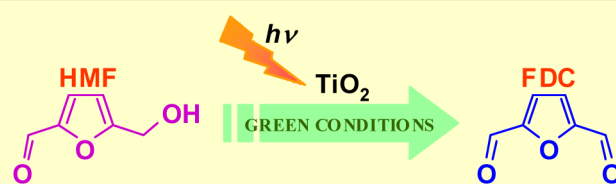
[†]Kimya Bölümü, Fen-Edebiyat Fakültesi, Afyon Kocatepe Üniversitesi, Ahmet Necdet Sezer Kampüsü, 03200, Afyon, Turkey
[‡]"Schiavello-Grillone" Photocatalysis Group, Dipartimento di Energia, Ingegneria dell'Informazione e Modelli Matematici (DEIM), Università degli Studi di Palermo, Viale delle Scienze (ed. 6), 90128 Palermo, Italy

S *Supporting Information*

ABSTRACT: 5-(Hydroxymethyl)-2-furaldehyde (HMF) was selectively oxidized to 2,5-furandicarbaldehyde (FDC) in aqueous medium by using home-prepared (HP) anatase, rutile, and brookite TiO$_2$ nanoparticles. HP samples were prepared via a sol−gel method by using TiCl$_4$ as the TiO$_2$ precursor. Commercial TiO$_2$ catalysts were also used for comparison. All samples were characterized by BET specific surface area, XRD, TGA, and SEM, and the reactivity results showed that HP catalysts are predominantly amorphous and give rise to selectivities toward FDC more than twice that of commercial and well-crystallized catalysts.

KEYWORDS: *5-(Hydroxymethyl)-2-furaldehyde, Selective oxidation, Photocatalytic synthesis, TiO$_2$, 2,5-Furandicarbaldehyde*

INTRODUCTION

Photocatalytic reactions have been generally applied to unselective transformations aimed at water and air remediation because they are carried out by means of radicals.[1,2] However, during the last few years, investigations have been performed in the field of photocatalytic synthesis as a green chemistry tool to be used in place of dangerous and polluting routes. Recently, some synthetic reactions, such as partial oxidation of alcohols,[3−5] alkenes,[6,7] and cyclohexanes[8,9] have been deeply studied. In addition, CO$_2$[10,11] and nitro-compound[12,13] reductions and other photocatalytic syntheses such as photo-methatesis of olefins,[14] methane couplings,[15] heterocyclic functionalizations,[16] and C−N[17] and C−C[18] bond formations could be given as some examples of photosynthesis. Photo-catalytic processes carried out in water and in the presence of air without employing harmful stoichiometric oxidants and/or catalysts could be referred to as "green", and they could be proposed as methods alternative to the traditional industrial ones. Among the various semiconductor materials tested as oxidation photocatalysts, TiO$_2$ has shown to be the most reliable due to its low cost, chemical inert property, high photostability, and photoactivity.[19]

5-(Hydroxymethyl)-2-furaldehyde (HMF) is a common species present in almost all sweets because sugars easily degrade to HMF. Moreover, many catalytic processes involving production of HMF from fructose,[20] glucose,[21] polysaccharides, and biomass feedstocks[22] have been recently investigated. It is therefore challenging to find efficient and green synthetic methods able to transform HMF, which is a common byproduct, to valuable species.

Whereas no photocatalytic oxidation of HMF to 2,5-furandicarbaldehyde (FDC) has been reported until now, the literature reports many investigations on the selective catalytic oxidation of HMF to FDC that is a widespread chemical needed to obtain many industrially relevant compounds. The catalytic process is generally carried out in organic solvents by using hydrogen peroxide or air as oxidants at high pressure and temperature,[23,24] although some mild processes have also been developed.[25−27] These processes exhibit high values of selectivity to FDC in the 60−99% range, but they do not satisfy the conditions of the "green" chemistry. The present investigation reports the first photocatalytic green oxidation of HMF to FDC. The reaction has been carried out in aqueous medium in a batch reactor by using home-prepared (HP) and commercial TiO$_2$ photocatalysts under near-UV irradiation. Three HP catalysts were prepared by sol−gel methods making use of TiCl$_4$ as a precursor. Degussa P25 (P25), Sigma-Aldrich (SA), and Merck TiO$_2$ were the commercial catalysts used.

MATERIALS AND METHODS

Catalyst Preparation and Characterization. *Preparation of Anatase TiO$_2$.* The details of catalyst preparation are reported elsewhere.[28] The precursor solution was obtained by adding 20 mL

of TiCl$_4$ (purity >97%, Fluka) dropwise under magnetic agitation to 200 mL of deionized water contained in a 500 mL beaker put inside an ice bath. After that, the beaker was sealed, and mixing was prolonged for 12 h at room temperature, eventually obtaining a clear solution. A total of 125 mL of the resulting solution was put inside a 250 mL round-bottomed flask fitted with a Graham condenser. The flask was heated at 373 K, magnetically stirred, and refluxed for 2 h; the reflux zero time has been taken as that for which the solution left its transparency. The obtained suspension was then dried at 323 K by means of a rotary evaporator machine (Buchi model M) working at 50 rpm in order to obtain the final powdered catalysts. The final home-prepared catalyst is hereafter indicated as HPA.

Preparation of Rutile TiO$_2$. The details of the catalyst preparation are reported elsewhere.[28] The precursor solution was obtained by adding 20 mL of TiCl$_4$ (>97%, Fluka) to 1000 mL of water contained in a volumetric flask (2 L). At the end of the addition, the resulting solution was stirred for 2 min by a magnetic stirrer, and then the flask was sealed and maintained at room temperature (ca. 298 K) for a total aging time of 6 days. After ca. 12 h of aging, the sol became almost transparent, and then after waiting a few (2 or 3) days, the precipitation process started. The solid powder, precipitated at the end of the whole treatment, was separated by centrifugation (20 min at 5000 rpm) and dialyzed several times with deionized water until a neutral pH was reached. Then the sample was again centrifuged and dried at room temperature. The final home-prepared catalyst is hereafter indicated as HPR.

Preparation of Brookite TiO$_2$. The details of the catalyst preparation are reported elsewhere.[29] In particular, brookite was obtained by hydrolysis of TiCl$_4$ in a diluted HCl solution. Fifteen milliliters of TiCl$_4$ (98%) was added dropwise to a solution containing 630 mL of water and 160 mL of concentrated hydrochloric acid (>36%). The solution obtained after continuous stirring was heated in a closed bottle and aged at 373 K in an oven for 48 h. The resultant precipitate was constituted by a mixture of pure rutile and brookite nanoparticles that were separated by peptization by removing many times the supernatant and adding water to restore the initial solution volume. After a few washings, a dispersion of brookite particles formed while the rutile phase remained as precipitate. The dispersion was recovered, and the washing treatment was repeated until the liquid on the solid rutile became transparent. The sol containing the brookite particles was dried at 323 K by means of a rotary evaporator machine in order to obtain the final powdered catalysts. The final home-prepared catalyst is hereafter indicated as HPB.

Catalysts Characterization. SEM measurements were performed by using an ESEM microscope (Philips, XL30) operating at 25 kV. A thin layer of gold was evaporated on the catalysts samples, previously sprayed on the stab and dried at room temperature. BET specific surface areas were measured by the single-point BET method using a Micromeritics Flow Sorb 2300 apparatus. Before the measurement, the samples were dried for 1 h at 373 K, for 2 h at 423 K, and degassed for 0.5 h at 423 K. Thermogravimetric analyses (TGA) were performed by using a Shimadzu equipment (model TG60H). The heating rate was 10 °C min^{-1} in static air, and the powder amount, put in open Pt crucible, was 12 mg for all the samples. X-ray diffractometry (XRD) patterns of the powders were recorded by a Philips diffractometer (operating at a voltage of 40 kV and a current of 30 mA) using the Cu Kα radiation and a 2θ scan rate of 1.28° min^{-1}.

The crystallinity of TiO$_2$ samples was evaluated by using the following procedure reported in the literature.[30] XRD diffractograms were recorded for a mixture of TiO$_2$ and CaF$_2$ (50%, w/w) and the areas of the 100% peaks of rutile (110), anatase (110), and CaF$_2$ (220) were determined. By comparing the ratio between the areas of (110) and (220) peaks to the ratio obtained by using the pure phase (0.90 and 1.25 for rutile and anatase, respectively), the amount of crystalline and amorphous phases present in the HPA and HPR samples was determined. This procedure was not used for HPB as no reference values are reported for the brookite TiO$_2$ crystalline phase.

^{1}H NMR spectra were recorded on a Varian Mercury 400, 400 MHz High Performance Digital FT-NMR spectrometer. Chemical shifts are reported in ppm from tetramethylsilane with the residual protic

solvent resonance as the internal standard (CHCl$_3$: δ = 7.27 ppm). Infrared (IR) spectra were recorded on a Perkin-Elmer Paragon 100 FT-IR spectrophotometer. The samples were suspended in diethyl ether. A drop of this suspension was deposited on the surface of a NaCl cell. The solvent was then evaporated, and the film formed on the cell was analyzed directly.

Photoreactivity Setup and Procedure. A Pyrex beaker of 250 mL (d × h: 6 cm × 10 cm) was used as a photoreactor. The suspension was irradiated by four fluorescent black lamps (Philips, 8 W) that emit at 365 nm. The distance between the lamps axis and the reactor axis was 6 cm. The radiation energy impinging on the external surface of reactor had an average value of 3.0 mW cm^{-2}. It was measured by using a radiometer (Delta Ohm, DO 9721). In the course of the photocatalytic runs, the temperature of the suspension was ca. 308 K. A magnetic stirrer guaranteed a satisfactory suspension of the photocatalyst and the homogeneity of the reacting mixture. The initial concentration of the used substrate and catalysts were 0.5 mM and 0.2 g L^{-1}, respectively. The photocatalytic experiments were carried out at neutral pH that was adjusted by using 0.1 M NaOH or H$_2$SO$_4$ solutions. A run was also performed by using HPA and adding methanol (50 mM) as the hole trap. The initial volume of suspension inside the photoreactor was 150 mL. The catalyst amount chosen for the photocatalytic runs was the lowest one for which the resulting suspension was able to absorb more than 95% of the impinging radiation. This choice guaranteed that all the catalyst particles were irradiated. Before switching on the lamp, the suspension was kept in a ultrasonic bath for 10 min and then mixed for 30 min at room temperature to reach the thermodynamic equilibrium. Before and during the run, the aqueous suspension was in contact with atmospheric air so that it has been assumed that the dissolved oxygen concentration was always in equilibrium with that of the atmosphere.

The HMF amounts adsorbed by the catalysts under dark conditions were always quite low, i.e., less than 2% of the starting HMF amount. During the run, samples of reacting suspension were withdrawn at fixed time intervals; they were immediately filtered through a 0.45 μm hydrophilic membrane (HA, Millipore) before being analyzed. The quantitative determination and identification of the species present in the liquid was performed by means of a Shimadzu HPLC (Prominence LC-20A model and SPD-M20A Photodiode Array Detector) equipped with a Phenomenex Synergi 4 μm Hydro-RP 80A column and working at 313 K. The eluent consisted of 60% methanol and 40% deionized water. The flow rate was 0.2 cm^3 min^{-1}. Retention times and UV spectra of the compounds were compared with those of the standards (Sigma Aldrich). TOC analyses were carried out by using a 5000 A Shimadzu TOC analyzer. All the chemicals used were purchased from Sigma Aldrich with a purity ≥97.0%.

A specific photocatalytic run was carried out in order to produce a measurable amount of FDC. To this aim the run was performed in a 50 mL reaction volume at an HMF initial concentration of 6 mM and 0.5 g·L^{-1} of HPB sample; this run lasted 4 h. The organic products present in the aqueous phase were extracted with diethyl ether and concentrated by a rotovapor apparatus. FDC was separated by column chromatography by using a silica support (Silicagel 60, Merck) and a mixture of hexane and ethyl acetate (4:1 v:v) as the mobile phase. 2.4 mg of the product were isolated as colorless solid (14% yield).

■ RESULTS AND DISCUSSION

Figure 1 shows XRD patterns of HP and commercial TiO$_2$ photocatalysts. The peaks assignable to anatase are those at 25.58°, 38.08°, 48.08°, and 54.58°. Those referring to rutile are at 27.5°, 36.5°, 41°, 54.1°, and 56.5°. Finally, the ones characteristic of brookite those at 25.3°, 30.9°, 46.3°, and 55.8°. The HP samples contained only one crystalline phase: anatase for HPA, rutile for HPR, and brookite for HPB. The commercial samples, on the other hand, consist of an anatase–rutile mixture (P25), pure rutile (SA), and pure anatase (Merck). It may be noted that peaks of commercial photocatalysts are well defined, while those of HP samples are
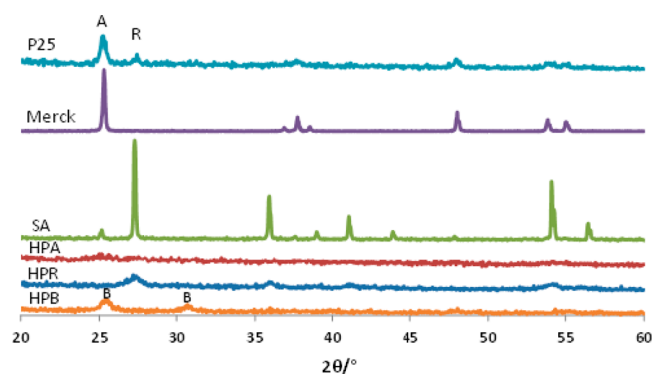
Figure 1. XRD patterns of HP and commercial TiO₂ photocatalysts.

Figure 2. TGA curves in air of SA, Merck, P25, HPB, HPR, and HPA.

broad and of low intensity, indicating a low degree of crystallinity.

All the information obtained by the textural characterization of catalysts is summarized in Table 1. The crystallinity of commercial samples is higher than 74%, while that of HP samples is less than ca. 13%. The values of crystallite sizes, determined by the Scherrer equation, indicate that with respect to the commercial catalysts the HP samples have smaller crystallites (3.6–10.9 nm vs 18–60 nm). All the HP samples were shown to be mesoporous. SEM measurements showed that the catalysts consist of agglomerates whose average diameters are lower (36–50 nm) for the HP samples than for the commercial ones (80–240 nm). BET specific surface areas of HP samples were found in the 70–189 m² g⁻¹ range; the commercial catalysts showed surface area values quite lower, in the 50–2.5 m² g⁻¹ range.

The TGA curves of all samples are shown in Figure 2. The HP samples showed a total weight loss of 11–25%. The loss between room temperature and 423 K was ca. 6–17%, and it may be attributed to the physically adsorbed water. No weight loss was observed by testing SA, while other commercial samples, Merck and P25, showed a low weight loss (Table 1). Table 1 also reports the calculated values of water physically adsorbed per unit surface area. Although the bulk properties of the samples were very different, it can be noted that the values of this parameter for the HP samples are higher than those of the commercial values. These results clearly indicate that the mainly amorphous HP samples are characterized by highly hydrophilic surfaces, whereas the mainly crystalline commercial samples have less hydrophilic surfaces. Notably a strict trend between physically adsorbed water and BET specific surface
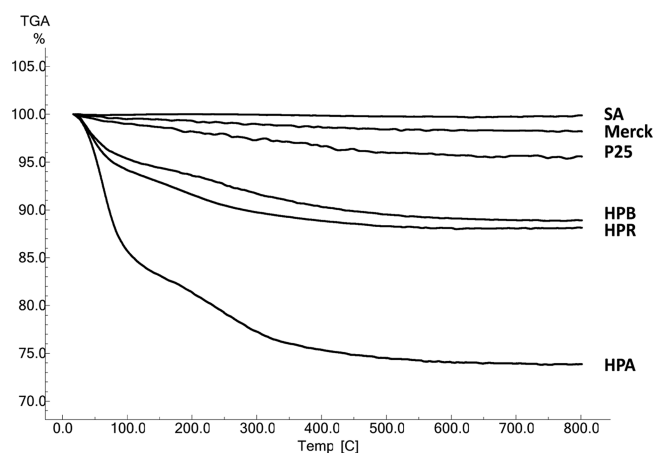
area can be observed, while there is an almost opposite trend between BET specific surface area and crystallinity, agglomerate sizes, and crystallite sizes. No reactivity of HMF was observed in the absence of irradiation, catalyst, or oxygen. Near-UV radiation, catalyst, and oxygen were needed for the occurrence of HMF conversion.

The results of representative runs carried out by using the HPB and P25 catalysts are reported in Figures 3 and 4, where
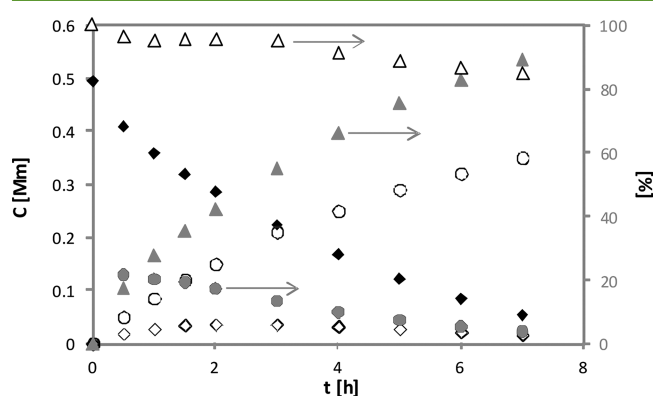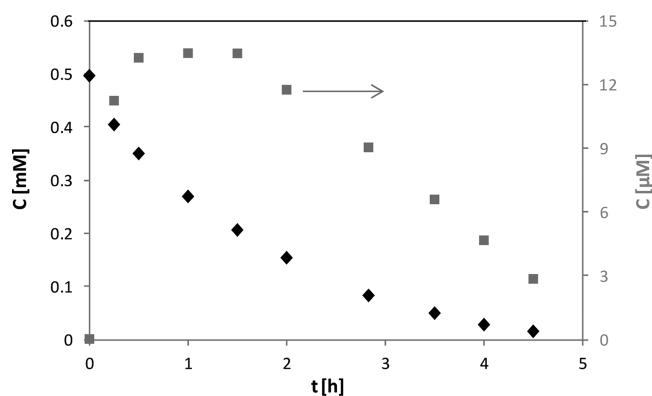

Figure 3. Experimental results of photocatalytic oxidation of HMF using HPB (0.2 g L⁻¹) catalyst. Symbols: concentrations of HMF (◆), FDC (◇), and CO₂ (○). Percentages of carbon mass balance (△), selectivity (gray ●) and conversion (gray ▲) are right quoted.

Table 1. Crystalline phase, crystallinity, physically adsorbed water, BET specific surface area (SSA), agglomerate size, and crystallite size of the catalysts and their photocatalytic performance for the oxidation of HMF to FDC[a]

catalyst	crystal phase[b]	crystallinity (%)	adsorbed water (mg m⁻²)	SSA (m² g⁻¹)	agglomerate size (nm)	crystal size (nm)	$r_0 \times 10^{6c}$ (mM m h⁻¹)	$t_{1/2}$[d] (h)	selectivity[e] (%)
SA	R	100	0	2.5	240	52	181	3.50	10.9
Merck	A	74	0.5	10	170	60	62	2.55	12.6
P25	A:R (80:20%)	90	0.5	50	80	26.5:18.2 (A:R)	28	1.15	12.0
HPB	B	–	0.7	70	50	10.9	8.2	2.60	21.0
HPR	R	12.8	0.7	105	36	6.8	2.2	13.0	25.0
HPA	A	2.85	0.9	189	45	3.6	2.4	3.95	22.5
HPA[f]	A	2.85	0.9	189	45	3.6	0.6	16.3	26

[a]Catalyst amount: 0.2 g L⁻¹. Initial HMF concentration: 0.5 mM. [b]A: anatase. R: rutile. B: brookite. [c]Initial reaction rate. [d]Irradiation time needed to reach a HMF conversion of 50%. [e]Selectivity = (produced FDC moles)/(converted HMF moles) × 100 at 20% conversion. [f]Run performed in the presence of 50 mM methanol.

Figure 4. Experimental results of photocatalytic oxidation of HMF using P25 (0.2 g L^{-1}). Symbols: concentration of HMF (◆) and FDC (gray ■). The latter values are right quoted.

the concentration values of HMF, FDC, and normalized CO_2 (TOC values divided by C HMF atoms) are reported versus the irradiation time. The values of HMF conversion and selectivity to FDC are also reported. During the run with HPB, the FDC concentration reached a maximum value when HMF conversion was ca. 50%, and then it continuously decreased. This decrease, quite slow for HPB but fast for P25, is likely due to over-oxidation of FDC.

In order to firmly state the presence of FDC as the product obtained by the HMF partial oxidation, a photocatalytic run aimed to obtain a measurable amount of that intermediate was carried out as described in the Materials and Methods section. The ^{1}H NMR analysis of the isolated compound gave the following figures for δ: 9.87 ppm (2H, s, COH) and 7.34 ppm (2H, s, Ar−H). These figures correspond to the commercial FDC standard. Other peaks present in NMR spectra (Figures S1, S2, Supporting Information) are due to the solvent. The FT-IR spectrum of the isolated FDC gave its characteristic peaks at 3110, 2980, 2840, 1676, 1413, 1270, and 1240 cm^{-1}. Also the UV−visible spectra, recorded by HPLC photodiode array, confirmed the identity of the formed FDC (Figure S3, Supporting Information).

An oxidation run aimed to investigate the further oxidation of FDC was performed with HPA and the P25 catalyst in the same experimental conditions used during HMF oxidation runs. The results showed that the FDC degradation occurred at a smaller rate than that found during HMF oxidation. Over-oxidation of FDC is therefore responsible for a decrease in selectivity at longer irradiation times. This effect was less important when the HP samples were used.

The quantitative parameters used for determining the photoactivity performances of catalysts have been the irradiation time needed to reach a HMF conversion of 50%, $t_{1/2}$, the selectivity, defined as the ratio between the produced FDC moles, and the converted HMF ones at $t = t_{1/2}$, and the initial reaction rate, r_0, calculated by the following equation

$$r_0 = -\frac{1}{S}\left(\frac{dN}{dt}\right)_0 = -\frac{V}{S}\left(\frac{dC}{dt}\right)_0 \qquad (1)$$

where N indicates the number of HMF moles, t the irradiation time, S the specific surface area, V the suspension volume, and C the HMF concentration. It must be noted that the value of r_0 is independent of the surface area of the catalyst, and therefore, it is a reliable parameter for evaluating the intrinsic activity of the catalyst surface.

The initial reaction rates were far higher for the commercial samples than for the HP ones. On the contrary, the most selective catalysts were the HP ones (21−25%), while the commercial samples showed selectivity values (10.9−12.6%) about half with respect to the commercial ones. These results seem to indicate that the reactivity increases by increasing the samples' crystallinity. On the contrary, the selectivity values indicate that the partial oxidation process should be favored by using a catalyst that is mainly constituted by amorphous phases; these last ones being probably responsible for the high hydrophilic nature of the samples surface, as shown by the HP samples. The higher reactivity and lower selectivity showed by the HPB sample with respect to HPA and HPR could be a clue that the crystallinity of this sample is higher than that of HPA and HPR.

Concerning the reactivity of HP samples, it is worth noting that generally the specific photoreactivity cannot be straightforwardly related for samples with different crystallinity. Moreover, the question of the surface structure sensitivity is until now open in photocatalytic oxidation. Only recently, by investigating the water oxidation on extended surfaces of anatase crystals, it has been concluded that the photoactivity is not sensitive to the surface structure of anatase[31] and that the morphology and electronic properties of anatase nanoparticles dictate the activity.[32] In the present case, the catalyst surface is very complex as the HP preparation conditions produce titania samples that predominantly contain amorphous phases (Table 1) together with highly defective crystals. Indeed, adsorption and diffusion of reagent species are facilitated in catalysts with a large specific surface area, then promoting a higher photocatalytic activity. However, defective sites effective onto the surface for electron−hole recombination are also present, and their density depends both on crystallinity and on the value of the specific surface area. Therefore, large specific surface area and low crystallinity, as those showed by HP samples, can determine the higher electron−hole recombination rate and, as a consequence, a worsening of the photocatalytic activity. In conclusion, the data of Table 1 clearly shows a strong dependence among crystallinity, selectivity, and initial reaction rate: a crystallinity decrease produces both a selectivity increase and a reaction rate decrease.

With the aim of improving the selectivity toward partial oxidation reaction, an aliphatic alcohols acting as hole trap was added to the reacting suspension. Small amounts of methanol with respect to water were used in a run carried out by using HPA as the catalyst; Figure 5 reports the relative experimental data. It was observed that a strong decrease in the reactivity was accompanied, however, by a small increase in the selectivity from 22.5% to 26% in respect to a similar run carried out in the absence of methanol (Table 1). These results indicate that in the methanol-containing photocatalytic system the aliphatic alcohol acts as an efficient hole trap by decreasing the overall degradation rate, but it affects in a more significant way the mineralization reaction as the selectivity increases.

The photocatalytic runs clearly indicated that the main oxidation products detected from the start of irradiation were FDC and CO_2; for a HMF conversion of 50%, no other intermediate compounds were detected, being the sum of FDC and CO_2 moles equal to ca. 95% of the reacted HMF moles. Even if in heterogeneous photocatalysis the mechanisms of partial oxidation reactions are not simple,[33] the photoreactivity results allow us to hypothesize that the HMF photocatalytic oxidation proceeds through two parallel pathways, both
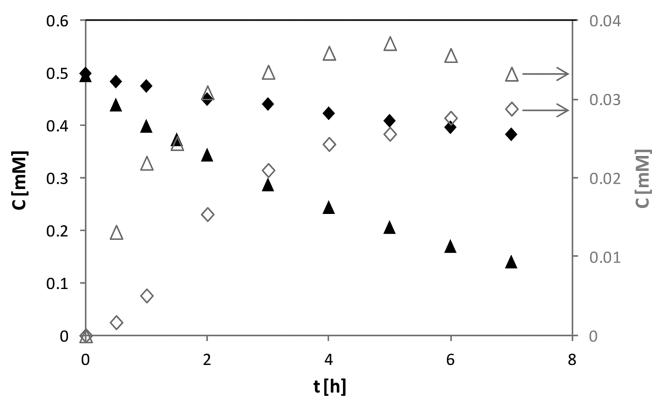
Figure 5. Experimental results of photocatalytic oxidation of HMF using the HPA (0.2 g L^{-1}) catalyst in the absence and in the presence of methanol (50 mM). Symbols: concentration of (◆) HMF and (◇) FDC in the presence of methanol and (▲) HMF and (△) FDC in the absence of methanol.

effective from the start of irradiation: (i) partial oxidation to FDC that is released into the liquid phase and subsequently may compete with HMF for further oxidation that eventually gives rise to mineralization and (ii) complete oxidation to CO_2 and H_2O through intermediates that do not desorb from the catalyst surface.[3,4] These two pathways involve two different sites.[34] The significantly higher selectivity to FDC on HP samples than on well-crystalline samples indicates that amorphous titania is providing more active sites for HMF partial oxidation.

Scheme 1 shows the hypothesized mechanism for HMF oxidation that takes place through adsorption and reaction on two different kinds of catalytic sites (one for partial oxidation and the other for mineralization). The route involving direct HMF mineralization is also reported and occurs without any desorption of intermediates. The first step of HMF partial oxidation to FDC is hypothesized to be brought to the alcoholic group by either a hole (h^+) or a hydroxyl radical. Upon this rate-determining step, the subsequent transformations involve the formation of a CHO group. O_2 could also play a role in producing oxidant species (for instance HO_2 radicals) by reacting with H_2O. It is worth noting that the starting five-membered ring HMF molecule is probably attacked and destroyed more easily than other aromatic six-membered ring molecules subjected to photocatalytic oxidation that can give rise to several hydroxylated species as
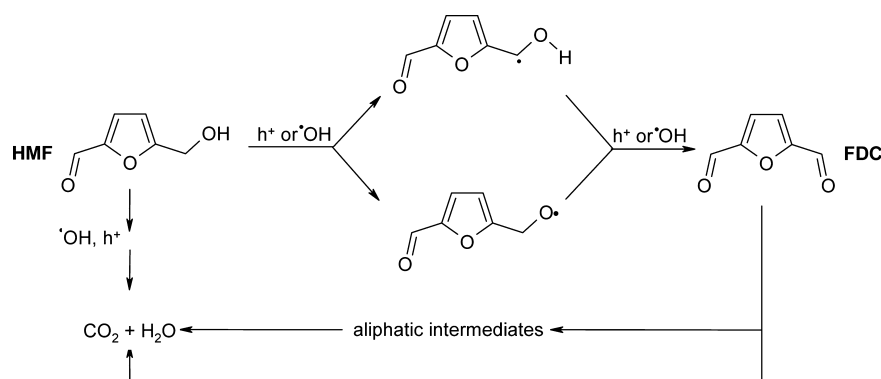
intermediates.[35] This statement can explain the absence of other oxidized species in solution throughout the process.

CONCLUSION

The common industrial byproduct HMF may be partially oxidized in aqueous medium through a photocatalytic process that can be considered totally "green" by obtaining as a unique product the corresponding aldehyde (FDC) that is a compound of industrial interest. Commercial TiO_2 samples showed to be much less selective (but more active) than poorly crystalline catalysts that gave rise to ca. 22% selectivities. The used crystalline allotropic phase did not seem to have a strong influence on the global selectivity of the process. It can be hence foreseen a scale-up of the presented process aiming to an industrial production after the optimization of all of the parameters, and for instance, the exploitation of a suitable membrane could be useful to selectively permeate FDC, avoiding its further oxidation and consequently improving the selectivity of the global process.

ASSOCIATED CONTENT

⊙ Supporting Information
Additional figures. This material is available free of charge via the Internet at http://pubs.acs.org.

AUTHOR INFORMATION

Corresponding Author
*E-mail: sedatyurdakal@gmail.com (S.Y.), vincenzo.augugliaro@unipa.it (V.A.).

Notes
The authors declare no competing financial interest.

ACKNOWLEDGMENTS

REFERENCES

(1) Hoffmann, M. R.; Martin, S. T.; Choi, W.; Bahnemann, D. W. Environmental applications of semiconductor photocatalysis. *Chem. Rev.* **1995**, *95*, 69−96.
(2) Augugliaro, V.; Bellardita, M.; Loddo, V.; Palmisano, G.; Palmisano, L.; Yurdakal, S. Overview on oxidation mechanisms of organic compounds in heterogenous photocatalysis. *J. Photochem. Photobiol. C: Photochem. Rev.* **2012**, *13*, 224−245.

Scheme 1

(3) Yurdakal, S.; Palmisano, G.; Loddo, V.; Augugliaro, V.; Palmisano, L. Nanostructured rutile TiO₂ for selective photocatalytic oxidation of aromatic alcohols to aldehydes in water. *J. Am. Chem. Soc.* **2008**, *130*, 1568−1569.

(4) Palmisano, L.; Augugliaro, V.; Bellardita, M.; Di Paola, A.; García López, E.; Loddo, V.; Marcì, G.; Palmisano, G.; Yurdakal, S. Selective oxidation in water by TiO₂ photocatalysis. *ChemSusChem* **2011**, *4*, 1431−1438.

(5) Higashimoto, S.; Kitao, N.; Yohida, N.; Sakura, T.; Azuma, M.; Ohue, H.; Sakata, Y. Selective photocatalytic oxidation of benzyl alcohol and its derivatives into corresponding aldehydes by molecular oxygen on titanium dioxide under visible light irradiation. *J. Catal.* **2009**, *266*, 279−285.

(6) Murata, C.; Yoshida, H.; Kumagai, J.; Hattori, T. Active sites and active oxygen species for photocatalytic epoxidation of propene by molecular oxygen over TiO₂−SiO₂ binary oxides. *J. Phys. Chem. B* **2003**, *107*, 4364−4373.

(7) Kluson, P.; Luskova, H.; Cerveny, L.; Klisakova, J.; Cajtham, T. Partial photocatalytic oxidation of cyclopentene over titanium(IV) oxide. *J. Mol. Catal. A: Chem.* **2005**, *242*, 62−67.

(8) Maldotti, A.; Molinari, A.; Amadelli, R.; Carbonell, E.; García, H. Photocatalytic activity of MCM-organized TiO₂ materials in the oxygenation of cyclohexane with molecular oxygen. *Photochem. Photobiol. Sci.* **2008**, *7*, 819−825.

(9) Ciambelli, P.; Sannino, D.; Palma, V.; Vaiano, V.; Mazzei, R. S.; Eloy, P.; Gaigneaux, E. M. Photocatalytic cyclohexane oxidehydrogenation on sulphated MoOₓ/γ-Al₂O₃ catalysts. *Catal. Today* **2009**, *141*, 367−373.

(10) Tan, S. S.; Zou, L.; Hu, E. Photocatalytic reduction of carbon dioxide into gaseous hydrocarbon using TiO₂ pellets. *Catal. Today* **2006**, *115*, 269−273.

(11) Shaohua, L.; Zhihuan, Z.; Zhizhong, W. Photocatalytic reduction of carbon dioxide using sol−gel derived titania-supported CoPc catalysts. *Photochem. Photobiol. Sci.* **2007**, *6*, 695−700.

(12) Kominami, H.; Iwasaki, S.; Maeda, T.; Imamura, K.; Hashimoto, K.; Kera, Y.; Ohtani, B. Photocatalytic reduction of nitrobenzene to aniline in an aqueous suspension of titanium(IV) oxide particles in the presence of oxalic acid as a hole scavenger and promotive effect of dioxygen in the system. *Chem. Lett.* **2009**, *38*, 410−411.

(13) Wang, H.; Yan, J.; Chang, W.; Zhang, Z. Practical synthesis of aromatic amines by photocatalytic reduction of aromatic nitro compounds on nanoparticles N-doped TiO₂. *Catal. Commun.* **2009**, *10*, 989−995.

(14) Inaki, Y.; Yoshida, H.; Hattori, T. Active sites on mesoporous and amorphous silica materials and their photocatalytic activity: an investigation by FTIR, ESR, VUV−UV and photoluminescence spectroscopies. *J. Phys. Chem. B* **2002**, *106*, 9098−9106.

(15) Yoshida, H.; Matsushita, N.; Kato, Y.; Hattori, T. Synergistic active sites on SiO₂−Al₂O₃−TiO₂ photocatalysts for direct methane coupling. *J. Phys. Chem. B* **2003**, *107*, 8355−8362.

(16) Gambarotti, C.; Punta, C.; Recupero, F.; Caronna, T.; Palmisano, L. TiO₂ in organic photosynthesis: sunlight induced functionalization of heterocyclic bases. *Curr. Org. Chem.* **2010**, *14*, 1153−1169.

(17) Selvam, K.; Krishnakumar, B.; Velmurugan, R.; Swaminathan, M. A simple one pot nano titania mediated green synthesis of 2-alkylbenzimidazoles and indazole from aromatic azides under UV and solar light. *Catal. Commun.* **2009**, *11*, 280−284.

(18) Iizuka, M.; Yoshida, M. Redox system for perfluoroalkylation of arenes and α-methylstyrene derivatives using titanium oxide as photocatalyst. *J. Fluorine Chem.* **2009**, *130*, 926−932.

(19) Fujishima, A.; Hashimoto, K.; Watanabe, T. *TiO₂ Photocatalysis, Fundamentals and Applications*; BKC, Inc.: Tokyo, 1999.

(20) Ilgen, F.; Ott, D.; Kralisch, D.; Reil, C.; Palmberger, A.; König, B. Conversion of carbohydrates into 5-hydroxymethylfurfural in highly concentrated low melting mixtures. *Green Chem.* **2009**, *11*, 1948−1954.

(21) Huang, R.; Qi, W.; Su, R.; He, Z. Integrating enzymatic and acid catalysis to convert glucose into 5-hydroxymethylfurfural. *Chem. Commun.* **2010**, *46*, 1115−1117.

(22) Cheda, J. N.; Roman-Leshkov, Y.; Dumesic, J. A. Production of 5-hydroxymethylfurfural and furfural by dehydration of biomass-derived mono- and poly-saccharides. *Green Chem.* **2007**, *9*, 342−350.

(23) van Deurzen, M. P. J.; van Rantwijk, F.; Sheldon, R. A. Chloroperoxidase-catalyzed oxidation of 5-hydroxymethylfurfural. *J. Carbohydr. Chem.* **1997**, *16*, 299−309.

(24) Moreau, C.; Durand, R.; Pourcheron, C.; Tichit, D. Selective oxidation of 5-hydroxymethylfurfural to 2,5-furan-dicarboxaldehyde in the presence of titania supported vanadia catalysts. *Stud. Surf. Sci. Catal.* **1997**, *108*, 399−406.

(25) Amarasekara, A. S.; Green, D.; McMillan, E. Efficient oxidation of 5-hydroxymethylfurfural to 2,5-diformylfuran using Mn(III)−salen catalysts. *Catal. Commun.* **2008**, *9*, 286−288.

(26) Ma, J.; Du, Z.; Xu, J.; Chu, Q.; Pang, Y. Efficient aerobic oxidation of 5-hydroxymethylfurfural to 2,5-Diformylfuran, and synthesis of a fluorescent material. *ChemSusChem* **2011**, *4*, 51−54.

(27) Carlini, C.; Patrono, P.; Raspolli Galletti, A. M.; Sbrana, G.; Zima, V. Selective oxidation of 5-hydroxymethyl-2-furaldehyde to furan-2,5-dicarboxaldehyde by catalytic systems based on vanadyl phosphate. *Appl. Catal., A* **2005**, *289*, 197−204.

(28) Yurdakal, S.; Augugliaro, V.; Loddo, V.; Palmisano, G.; Palmisano, L. Synthesis of p-anisaldehyde in water by N-doped TiO₂ photocatalyst under solar light irradiation. *New J. Chem.* **2012**, *36*, 172−178.

(29) Bellardita, M.; Di Paola, A.; Palmisano, L.; Parrino, F.; Buscarino, G.; Amadelli, R. Preparation and photoactivity of samarium loaded anatase, brookite and rutile catalysts. *Appl. Catal., B* **2011**, *104*, 291−299.

(30) Jensen, H.; Joensen, K. D.; Jørgensen, J. E.; Pedersen, J. S.; Søgaard, E. G. Characterization of nanosized partly crystalline photocatalysts. *J. Nanopart. Res.* **2004**, *6*, 519−526.

(31) Li, Y.-F.; Liu, Z.-P.; Liu, L.; Gao, W. Mechanism and activity of photocatalytic oxygen evolution on titania anatase in aqueous surroundings. *J. Am. Chem. Soc.* **2010**, *132*, 13008−13015.

(32) Li, Y.-F.; Liu, Z.-P. Particle size, shape and activity for photocatalysis on titania anatase nanoparticles in aqueous surroundings. *J. Am. Chem. Soc.* **2011**, *133*, 15743−15752.

(33) Li, Y.-F.; Liu, Z.-P. Dual reaction channels for photocatalytic oxidation of phenylmethanol on anatase. *Phys. Chem. Chem. Phys.* **2013**, *15*, 1082−1087.

(34) Yurdakal, S.; Palmisano, G.; Loddo, V.; Alagöz, O.; Augugliaro, V.; Palmisano, L. Selective photocatalytic oxidation of 4-substituted aromatic alcohols in water with rutile TiO₂ prepared at room temperature. *Green Chem.* **2009**, *11*, 510−516.

(35) Bellardita, M.; Augugliaro, V.; Loddo, V.; Megna, B.; Palmisano, G.; Palmisano, L.; Puma, M. A. Selective oxidation of phenol and benzoic acid in water via home-prepared TiO₂ photocatalysts: Distribution of hydroxylation products. *Appl. Catal., A* **2012**, *441−442*, 79−89.